

Sizing up the population of gamma-ray binaries

Guillaume Dubus¹, Nicolas Guillard², Pierre-Olivier Petrucci¹, and Pierrick Martin³

¹ Univ. Grenoble Alpes, CNRS, Institut de Planétologie et d'Astrophysique de Grenoble (IPAG), F-38000, Grenoble, France

² European Southern Observatory, Karl-Schwarzschild-str. 2, D-85748 Garching, Germany

³ Univ. Paul Sabatier, CNRS, Institut de Recherche en Astrophysique et Planétologie (IRAP), F-31028, Toulouse Cedex, France

Received ; accepted ; in original form February 1, 2022

ABSTRACT

Context. Gamma-ray binaries are thought to be composed of a young pulsar in orbit around a massive O or Be star, with their gamma-ray emission powered by pulsar spindown. The number of such systems in our Galaxy is not known.

Aims. We aim to estimate the total number of gamma-ray binaries in our Galaxy and to evaluate the prospects for new detections in the GeV and TeV energy range, taking into account that their gamma-ray emission is modulated on the orbital period.

Methods. We model the population of gamma-ray binaries and evaluate the fraction of detected systems in surveys with the *Fermi*-LAT (GeV), HESS, HAWC and CTA (TeV) using observation-based and synthetic template lightcurves.

Results. The detected fraction depends more on the orbit-average flux than on the lightcurve shape. Our best estimate for the number of gamma-ray binaries is 101^{+89}_{-52} systems. A handful of discoveries are expected by pursuing the *Fermi*-LAT survey. Discoveries in TeV surveys are less likely. However, this depends on the relative amounts of power emitted in GeV and TeV domains. There could be as many as ≈ 200 HESS J0632+057-like systems with a high ratio of TeV to GeV emission compared to other gamma-ray binaries. Statistics allow for as many as three discoveries in five years of HAWC observations and five discoveries in the first two years of the CTA Galactic Plane survey.

Conclusions. Continued *Fermi*-LAT observations are favoured over ground-based TeV surveys to find new gamma-ray binaries. Gamma-ray observations are most sensitive to short orbital period systems with a high spindown pulsar power. Radio pulsar surveys (SKA) are likely to be more efficient in detecting long orbital period systems, providing a complementary probe into the gamma-ray binary population.

Key words. Surveys – pulsars: general – Galaxy: stellar content – Gamma rays: stars – X-rays: binaries

1. Introduction

Gamma-ray binaries are systems composed of a massive star in orbit with a compact object, characterized by broad non-thermal emission peaking (in νF_ν) at energies above 1 MeV. The latter feature distinguishes them from high-mass X-ray binaries (HMXBs), whose spectral energy distribution peaks in X-rays, whereas the former distinguishes them from recycled binary millisecond pulsars, which have a low-mass companion. The compact object in gamma-ray binaries is likely to be a young, rotation-powered neutron star, with the non-thermal radiation due to the interaction of energetic pulsar wind particles with the stellar wind and radiation field of the O or Be companion. There is ample indirect evidence for this “binary pulsar wind nebula” scenario even though scattering in the stellar wind prevents detection of the expected radio pulsar in most gamma-ray binaries (see Dubus 2013 for a review). Accordingly, we explicitly assume in the following that the compact object in gamma-ray binaries is a pulsar. However, many of our results are equally applicable if the gamma-ray emission is powered by non-thermal jet emission from an accreting black hole (e.g. Massi et al. 2017). Clear evidence for gamma-ray jet emission exists for the accreting sources Cyg X-1 and Cyg X-3 but they are not gamma-ray binaries according to our definition because they are orders-of-magnitude more luminous in X-rays than in gamma rays.

There are six gamma-ray binaries detected in high (HE, 0.1–100 GeV) or very high energy (VHE, >100 GeV) gamma rays. Of these, two were initially detected as HE gamma-ray sources

in all-sky surveys (LS I +61°303, Gregory & Taylor 1978, and 1FGL J1018.6–5856, Ackermann et al. 2012), two were independently detected in HE gamma rays and X-rays before the association was made (LS 5039, Paredes et al. 2000, and LMC P3, Corbet et al. 2016), one was detected serendipitously in VHE observations of the Monoceros Loop (HESS J0632+057, Hinton et al. 2009), and one was detected in a radio pulsar survey (PSR B1259–63, Johnston et al. 1992). Follow-up observations established that these sources are binaries harbouring a massive star and that their non-thermal emission is modulated on the orbital period. In addition to those six gamma-ray binaries there are also four systems discovered in radio surveys with a young pulsar in orbit with a massive star, but where variable gamma-ray emission associated with the binary has yet to be detected because of the low pulsar power, long orbital timescale, and/or large distance: PSR J0045–7319, PSR J1638–4725, PSR J1740–3052 and PSR J2032+4127 (see Stairs et al. 2001; Bassa et al. 2011; Madsen et al. 2012; Lyne et al. 2015 respectively).

Gamma-ray binaries are probably a short-lived phase in the evolution of massive star binaries, following the birth of the neutron star and preceding the HMXB phase, when the neutron star accretes material captured from the stellar wind instead of holding it back (see Tauris & van den Heuvel 2006 for a review on the formation of compact objects in binaries). Accretion occurs if the ram pressure from accreting matter is able to overcome the pulsar wind, turning off the pulsar mechanism (Shvartsman 1971; Illarionov & Sunyaev 1975; Lipunov et al. 1994; Campana et al. 1995). A gamma-ray binary can thus transition to a HMXB on

the typical spindown timescale of young pulsars, a few 10^5 years. The evolution of the companion eventually leads to a second supernova with the formation of another compact object. Therefore, besides the unique opportunities they provide to understand the physics of pulsar winds, gamma-ray binaries also offer a window into the pulsar and orbital parameters of systems that remain bound after a supernova, and constrain the formation paths to double neutron stars and coalescing compact objects.

Achieving these goals depends on our ability to explore the population of gamma-ray binaries. The number of gamma-ray binaries in our Galaxy has been estimated from a few dozen to a few thousand systems from population synthesis studies of HMXB evolution (Meurs & van den Heuvel 1989; Iben et al. 1995; Portegies Zwart & Verbunt 1996; Portegies Zwart & Yungelson 1998). Gamma-ray binaries are more likely to stand out in gamma rays rather than in radio, optical or X-ray surveys where they are usually inconspicuous. The discovery of LMC P3 in the Large Magellanic Cloud suggests that we may have already accessed most of the observable gamma-ray binary population in our own Galaxy (Corbet et al. 2016).

Here, we aim to provide the first detailed estimate of the number of gamma-ray binaries based on HE and VHE observations and to evaluate the prospects for further discoveries. To do this, we simulate observations of gamma-ray binaries to assess the probability of detections in mock gamma-ray surveys, designed to follow as closely as possible those performed or planned with the *Fermi*-LAT, HESS, HAWC and CTA (§2). One difficulty in assessing the detectability is that the gamma-ray flux can vary strongly with orbital phase. We use input gamma-ray orbital lightcurves based on templates constructed from observations (§3) or on a radiative model (§4). The estimated population size and expectations for future detections are discussed in §5.

2. Simulating surveys

We simulate a measurement as the flux average of the gamma-ray binary lightcurve integrated over a certain duration and energy range. The duration of the measurement, the number of measurements (visits) and their distribution throughout time, varies according to the type of instrumentation. The observability and the detectability of the system will depend on the assumptions made for each type of survey that will be simulated. The observability depends only on the part of the sky surveyed and the location of the binary system. The detectability depends on the sensitivity of the survey, the cadence of the visits, and the emission properties of the system.

We simulate five types of surveys with properties as close as possible to existing or envisioned surveys, without carrying out a full end-to-end simulation of the observations and of the data analysis chain: in our opinion, current knowledge on the radiative mechanisms in gamma-ray binaries does not justify performing such complex and costly end-to-end simulations. The level of detail in our mock surveys is appropriate for the basic emission model that we develop in §4, which represents gamma-ray binary spectra at 1 GeV and 1 TeV with mono-energetic electrons. In the GeV domain, we simulate the *Fermi*-LAT third catalogue ("3FGL-like") and the *Fermi* All-sky Variability Analysis ("FAVA-like"). In the TeV domain, we simulate the HESS Galactic Plane survey ("HESS-like"), a "HAWC-like" survey, and the CTA Galactic Plane survey ("CTA-like"). A source is considered detected if its average flux in $\text{ph cm}^{-2} \text{s}^{-1}$ during the observation exceeds the threshold of the survey as defined below. We do not address the issue of how the detected gamma-ray source is identified as a gamma-ray binary, presumably through multi-

wavelength follow-up observations. In particular, we make no attempt to investigate how binaries can be identified through a period analysis, like the one performed on the *Fermi*-LAT catalog by Ackermann et al. (2012). Here, the orbital modulation only intervenes as the source of flux variability between observation windows.

2.1. The 3FGL-like survey

This survey tests whether the binary would have been included in the third *Fermi*-LAT catalogue (Acero et al. 2015). The whole Galactic Plane is covered so the gamma-ray binary observability is 100%. The measurement is assumed to last four years, ignoring any time variation in exposure. The threshold for detection is taken to be $10^{-9} \text{ ph cm}^{-2} \text{s}^{-1}$ (1-100 GeV) based on the flux distribution of sources detected within 10° of the Galactic Plane in Acero et al. (2015) (see their figure 24). We set the energy threshold at 1 GeV because the high-energy component of binaries peak around this energy and because the Galactic diffuse emission, which we do not take into account, is weaker than at 100 MeV. The 3FGL catalogue includes LS 5039, LS I +61°303, and 1FGL J1018.6-5856. LMC P3 is also part of the catalogue but is confused with other sources in the LMC. We also consider, where indicated, the impact of continued *Fermi*-LAT observations in the future. This "extended" 3FGL survey assumes a detection threshold lowered by a factor 2 and an exposure increased by a factor 4 (16 years of observations).

2.2. The FAVA-like survey

This is based on the search for 5.5σ deviations from a long-term average model of the GeV emission observed with the *Fermi*-LAT (Abdollahi et al. 2016). Following the FAVA procedure, deviations are searched for on a weekly timescale, which sets the duration of the simulated measurement, over a time span of 8 years. Again, any time-variation of the exposure is ignored and observability is 100%. The system is considered detected by this survey if its weekly average flux minus its long-term average flux (over 8 years) is greater than $10^{-6.5} \text{ ph cm}^{-2} \text{s}^{-1}$ (>100 MeV). Although the exact threshold changes as a function of location in the Galactic Plane and spectrum, this choice should be conservative based on Fig. 4 of Abdollahi et al. (2016). The FAVA survey is potentially more sensitive than the 3FGL survey to systems like PSR B1259-63 with long orbital periods and short duty cycles for GeV emission. The second FAVA catalogue includes LS I +61°303 and PSR B1259-63.

2.3. The HESS-like survey

This is based on the survey of the Galactic Plane carried out by the HESS collaboration since 2004 and is meant to be representative of what current imaging arrays of Cherenkov telescopes (IACTs) can achieve. The survey covers only part of the Galactic Plane, $-110^\circ \leq l \leq 65^\circ$. The observability of a system is decided by checking that it is observable for at least two hours at some point in the year at a zenith angle smaller than 45° , assuming the geographical location of the HESS array, and that its longitude is within the surveyed area. To produce a schedule of observations, we randomly distributed 25 visits of 2 hours over a time span of 8 years i.e. we assume a uniform survey exposure of 50 hours is achieved. We take into account that observations occur at night, ensuring each binary has a preferred observation season. However, we do not account for Moon-less operations, which influences

the distribution of observable time on a monthly timescale. The latter effect averages out over a timescale of a few years, whereas the former (preferred season) does not. The measured fluxes from each visit are then averaged and compared to a detection threshold of $3.6 \times 10^{-13} \text{ ph cm}^{-2} \text{ s}^{-1}$ ($>1 \text{ TeV}$). This threshold corresponds to a flux of 20 mCrab¹. The exposure times and sensitivity are comparable to those of the HESS survey². We also considered whether a detection could be claimed from a single visit, scaling the threshold by a factor $(50/2)^{1/2}$.

2.4. The CTA-like survey

The CTA-like survey is intended to test the potential performance of the CTA array in detecting new gamma-ray binaries. The guiding principles are identical to the HESS-like survey. We assume that the survey is divided up into two blocks carried out in parallel during the first two years of operations, based on the plans for an initial Galactic Plane survey by the CTA consortium (Vercellone 2017). The first block, carried out by the South array in Chile, covers longitudes $-60^\circ \leq l \leq 60^\circ$ down to a sensitivity of 2.7 mCrab using 6 visits of 2 hours. The second block, carried out by the North array in the Canary Islands, covers $60^\circ \leq l \leq 150^\circ$ down to 4.2 mCrab in 4 visits of 2 hours. We also consider the “full” survey covering all the Galactic Plane and carried out over a timespan of 10 years (see Fig. 6 in Vercellone 2017 for details). The observability of each system is decided as for the HESS-like survey using the planned locations for the arrays.

2.5. The HAWC-like survey

Finally, we tested for the detection of binaries using the extended air shower array HAWC. The high duty cycle and full-sky monitor capacity of HAWC can make it more sensitive to flaring gamma-ray binaries than IACTs like HESS and CTA. Here, the binary is observable if it transits with a zenith angle smaller than 45° at the location of the HAWC array in Mexico. We then simulate one measurement per day at the time of transit and with a duration equal to transit duration. The HAWC sensitivity after five years of operation is comparable to that achieved in the HESS Galactic Plane survey, 20 mCrab above 1 TeV, assuming a source transit duration across the sky of six hours (Carramiñana 2016). The threshold for daily detection is close to 1 Crab for a 6-hour transit, corresponding to the transit time of a source that passes close to zenith *i.e.* with a declination close to $+19^\circ$. The dependence of the threshold with source declination is taken into account by using the curve showing sensitivity as a function of declination for a $E^{-2.5}$ spectrum in Fig. 10 of Abeysekara et al. (2017). We test for detection in each daily measurement and in the accumulated exposure over 5 years of HAWC operations.

3. Extrapolating from observed gamma-ray binaries

We currently have five binaries with measured orbital modulations at both GeV and TeV energies and one with a GeV modulation (LMC P3). How sensitive are the surveys to the detection of these binaries? This is estimated here by constructing a template lightcurve for each of the known gamma-ray binaries and, after

proper scaling for distance, deriving the probability for detection once the binary is randomly located in the Galaxy.

3.1. Template lightcurves

Figure 1 shows template lightcurves for each of the known gamma-ray binaries based on the GeV and TeV observations available at the time of writing. In most cases, we simply took the phase-folded measurements and interpolated using splines. For PSR B1259-63, LS I +61°303, and HESS J0632+057, the error bars, phase coverage, or orbit-to-orbit variations make it difficult to assess the mean orbital lightcurves. In these cases, our templates are meant to be representative of the behaviour of the system in that they roughly capture the amplitude and phase variations that have been observed. The template GeV and TeV lightcurves are given in $\text{ph cm}^{-2} \text{ s}^{-1}$, integrated above 1 GeV and 1 TeV (respectively). We converted to these units assuming a simple power-law when the data was not directly available in this format. The source of the data and the power-law photon index Γ (with $dN \propto E^{-\Gamma} dE$) that we used can be found in the caption to Fig. 1. Given the low statistics, the GeV lightcurve of HESS J0632+057 (not shown in Fig. 1) is described as a two bin lightcurve (orbital phases 0.0-0.5 and 0.5-1.0) using the spectral parameters in Tab. 1 of Li et al. (2017), who report the first detection of this system at GeV energies³.

Table 1 lists the detected systems for each mock survey presented in §2, given the template lightcurves and locations of the known binaries in the Galaxy. LS I +61°303 is not detected in the HESS-like survey due to its location. LS 5039 and LS I +61°303 are observable with HAWC but undetected due to their unfavorable declinations, in agreement with the 18 months of HAWC observations that have been reported to date (Abeysekara et al. 2017). PSR B1259-63 is always detected in the FAVA survey. The system is just below the threshold of the 3FGL survey when the four-year survey timespan includes only one periastron passage of the 3.4 yr orbit, as observed. PSR B1259-63 has a very small probability ($< 1\%$) of being detected in the HESS survey due to its low duty cycle and flux, but a 50% chance of being detected in the CTA-like survey. HESS J0632+057 is outside the HESS and initial CTA-like surveys; it is detected in the full CTA survey. 1FGL J1018.6-5856 is detected only in the 3FGL-like survey and in the full CTA-like survey. LMC P3 is detected only in the 3FGL-like survey. These results are fully consistent with the actual 3FGL, FAVA, and HESS survey observations.

3.2. Galactic distribution

We assume that gamma-ray binaries are located in or close to the spiral arms of our Galaxy, like O and B stars and the HMXBs to which they are directly related. The Galaxy is modelled as four one-dimension spiral arms. We use the arm formula of Rindermacher & Mead (2009) with parameters adjusted to reproduce the Galactic structure in Figure 5 of Russeil (2003). Our Sun is 8 kpc away from the Galactic Center. Binaries are spread out uniformly across the Galaxy disk (15 kpc), keeping only those within 1 kpc of a spiral arm and more than 3 kpc away from the Galactic Center (to account for the older stellar population in the bulge, see Fig. 2). The binaries are assumed to reside in the Galactic Plane ($b = 0^\circ$). The model Galactic longitude distribu-

¹ For the VHE surveys, we have converted Crab units to integrated flux above 1 TeV using $1 \text{ Crab} \equiv 1.82 \times 10^{-11} \text{ ph cm}^{-2} \text{ s}^{-1}$, based on the Crab spectrum measured by Albert et al. (2008).

² <https://www.mpi-hd.mpg.de/hfm/HESS/pages/home/som/2016/01>

³ The *Fermi*-LAT detection reported by Malyshev & Chernyakova (2016) is compatible with the detection of the low-energy end of the VHE spectrum rather than the detection of a distinct GeV spectral component as in the other gamma-ray binaries.

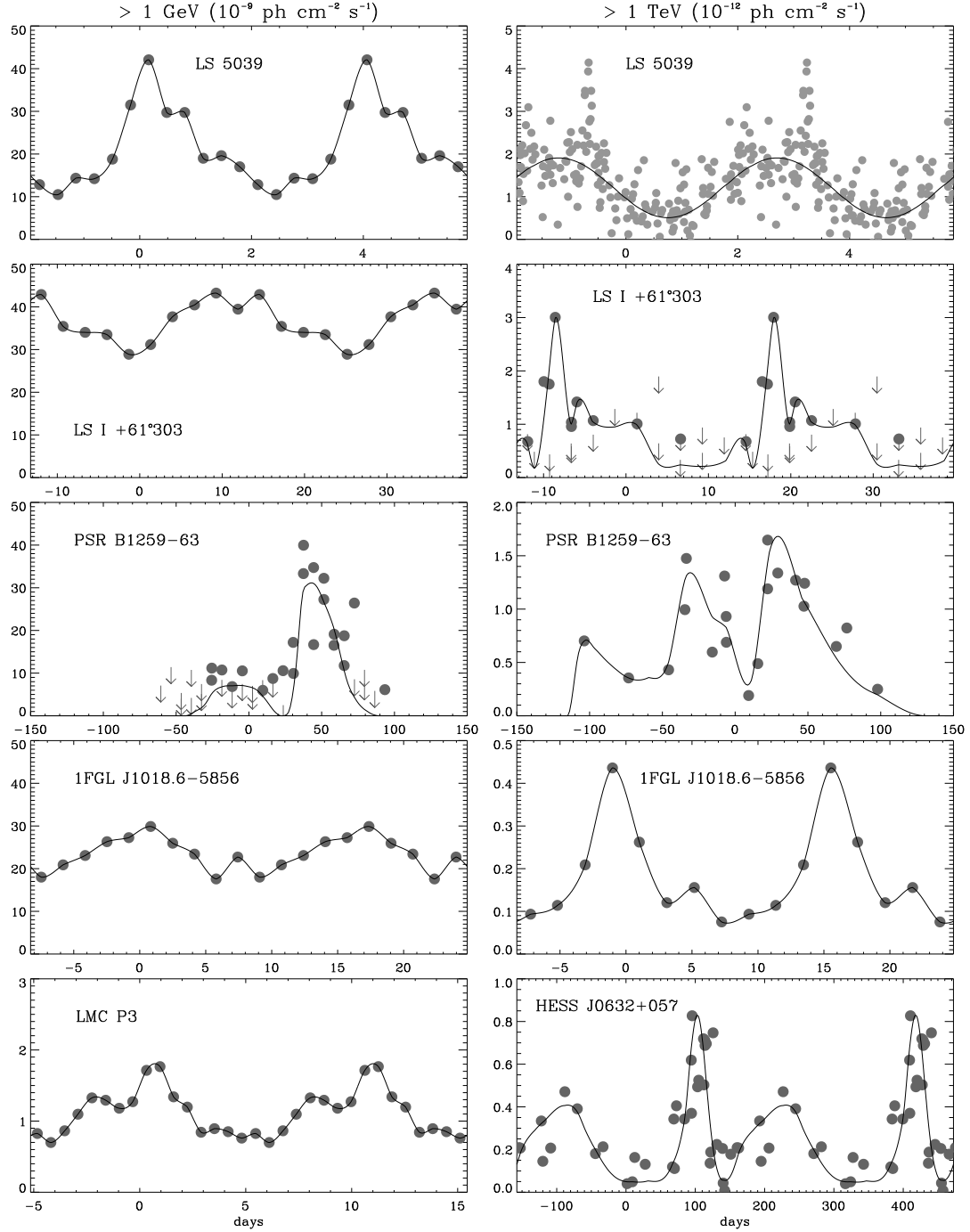


Fig. 1. Template lightcurves for known gamma-ray binaries. Two orbits are shown except for PSR B1259-63 where the plot focuses on periastron passage. The various measurements are shown in grey, with error bars omitted for clarity. Arrows indicate measurement upper limits. Left: photon flux integrated above 1 GeV in units of $10^{-9} \text{ ph cm}^{-2} \text{ s}^{-1}$ based on *Fermi*-LAT measurements. Right: photon flux integrated above 1 TeV in units of $10^{-12} \text{ ph cm}^{-2} \text{ s}^{-1}$ based on IACT measurements. The GeV and TeV data are taken from [Abdo et al. \(2009\)](#) and [Aharonian et al. \(2006\)](#) for LS 5039 with $\Gamma_{\text{GeV}} = 2.54$; [Hadasch et al. \(2012\)](#) and [Acciari et al. \(2011\)](#) for LS I +61°303, with $\Gamma_{\text{GeV}} = 2.42$ and $\Gamma_{\text{TeV}} = 2.6$; [Bordas et al. \(2016\)](#) for PSR B1259-63, with $\Gamma_{\text{GeV}} = \Gamma_{\text{TeV}} = 2.7$; [Ackermann et al. \(2012\)](#) and [Abramowski et al. \(2015\)](#) for 1FGL J1018.6-5856, with $\Gamma_{\text{GeV}} = 3.1$ and $\Gamma_{\text{TeV}} = 2.7$. The GeV data for LMC P3 is from [Corbet et al. \(2016\)](#) with $\Gamma_{\text{GeV}} = 2.8$. The TeV data for HESS J0632+057 is from [Aliu et al. \(2014\)](#).

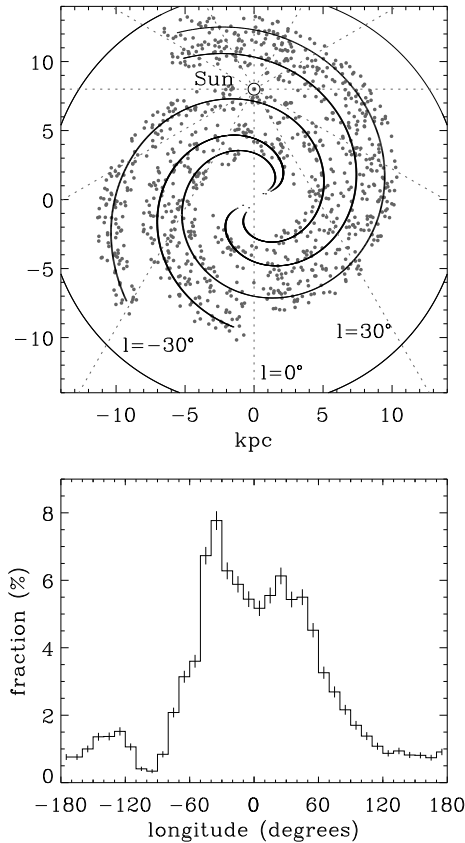
tion (Fig. 2) compares well to the HMXB longitude distribution plotted in [Grimm et al. \(2002\)](#) or [Walter et al. \(2015\)](#).

The ground-based surveys (HESS, HAWC, initial CTA) access only part of the Galactic Plane, hence only a fraction of the binaries are observable for them. These fractions are given in Tab. 2 for both a distribution along spiral arms, as described

above, and a strictly uniform disk distribution. This makes little difference. In the following, we considered only the spiral arm distribution.

Table 1. Detected systems in the mock surveys based on the template lightcurves in Fig. 1.

mock survey	detected system
3FGL	LS 5039, LS I +61°303, 1FGL J1018.6-5856, LMC P3
FAVA	LS I +61°303, PSR B1259-63
HESS	LS 5039
HAWC	none
CTA	LS 5039, LS I +61°303, PSR B1259-63
CTA (full)	LS 5039, LS I +61°303, PSR B1259-63, HESS J0632+057, 1FGL J1018.6-5856

**Fig. 2.** Top: map of randomly-generated locations for gamma-ray binaries in the Galaxy. Bottom: longitude distribution of gamma-ray binaries under the assumptions described in §3.2.**Table 2.** Fraction (%) of observable binaries in each survey.

	HESS	HAWC	CTA
spiral	72.25±0.28	55.85±0.31	82.94±0.23
disk	75.26±0.27	52.44±0.31	80.94±0.24

3.3. Detectable fraction based on observed lightcurves

Table 3 reports the detectable fraction of gamma-ray binaries in the various surveys, based on a sample of 10^4 systems randomly distributed in Galactic location and in starting orbital phase for each template lightcurve in Fig. 1 after scaling for distance. The lightcurves are then run through the simulated observations of each survey described in §2 to test for detection. For example, the 3FGL-like survey detects $77.9 \pm 0.8\%$ of the binaries that are

assumed to have a GeV lightcurve identical to LS 5039. Here and in the remainder of the paper, the errors represent the 95% confidence interval derived from a likelihood analysis⁴.

1FGL J1018.6-5856 and LMC P3 have high enough luminosities that such systems are detectable anywhere in the Galaxy with the 3FGL survey. Unsurprisingly, the FAVA-like survey is best-suited for low duty cycle lightcurves like PSR B1259-63. Our analysis recovers that PSR B1259-63 is detected in FAVA, but would not include LS I +61°303. The latter is inconsistent with the FAVA catalogue and is the result of neglecting the orbit-to-orbit variations that are detected in this source (Ackermann et al. 2013). The FAVA-like analysis also fails to detect LS 5039 and 1FGL J1018.6-5856 since the amplitude of the flux variations on weekly timescales are insufficient to flag them. In this case, this is consistent with the actual FAVA results (Abdollahi et al. 2016).

The numbers remain small in the HESS and HAWC-like surveys. It is only with CTA that detection fractions comparable to those achieved by the *Fermi*-LAT will be possible due to the high sensitivity of the instrument. Very few systems are detected as transients in the ground-based surveys (*i.e.* detected only in one visit): the flux increase compared to the average in a highly eccentric system rarely compensates the higher sensitivity threshold for observations on a shorter duration. Hence, the fraction of detected systems in VHE surveys decreases with longer orbital period even if the systems have comparable maximum TeV luminosities due to a high eccentricity.

The fractions in Tab. 3 give an estimated detection probability from which we can constrain the maximum size of the underlying population⁵. Any other existing system with identical properties to 1FGL J1018.6-5856 or LMC P3 would have been detected since the detection probability is 1. For LS 5039, knowing that the system is detected in the 3FGL survey, the 77.9% probability implies with >95% confidence that there is at most three systems with comparable lightcurves in our Galaxy and most likely only one. The same conclusion is reached for LS I +61°303. For PSR B1259-63, given the FAVA detection, the 12.6% detection probability implies 7_{-6}^{+26} such systems in our Galaxy. Therefore, on average, there may be one more LS 5039 or LS I +61°303 type

⁴ Here, we estimate the probability p to detect a binary in a survey. We find m detections after running a random sample of n systems through our mock survey procedure. The likelihood function is $L(p) = C_n^m p^m (1-p)^{n-m}$, where C_n^m is the binomial coefficient. The function has a maximum L_m for $p = m/n$. Defining the test statistic as $T = 2 \log(L_m/L)$ and applying Wilks' theorem, the 95% confidence interval on p is calculated from the interval where $T \leq 3.84$ (the cutoff value in a χ^2 distribution with one degree of freedom beyond which the probability $\leq 5\%$). The chosen number of systems n to simulate is a compromise between computational time and statistical error.

⁵ We take the detection probability p derived by the simulation and find the population n that maximises the likelihood (see footnote 4) to detect m observed systems. Here, $m = 1$ for each type of gamma-ray binary.

system, and 6 other PSR B1259-63-like systems in the Galaxy that could have escaped detection in the *Fermi*-LAT data.

The VHE detection probabilities are not as constraining as the HE ones except for HESS J0632+057. The detection probability is only 0.8% in both the 3FGL and HESS-like surveys. The lack of detection in those surveys (note that HESS J0632+057 is outside the HESS survey area, §3.1) places an upper limit of <231 on the number of HESS J0632+057-like systems in the Galaxy. The initial CTA-like survey should detect 11^{+8}_{-6} of those 231 systems, or will reduce their estimated number to 8^{+30}_{-7} should it detect only HESS J0632+057 after the full 10 year Galactic Plane survey. CTA will thus be able to strongly constrain the number of such systems.

4. A synthetic population

In the preceding section we estimated the number of existing gamma-ray binaries from the properties of the known systems. However, these systems represent only the upper end of the luminosity function of gamma-ray binaries. In this section we will estimate this number from a synthetic population model. Building this population requires a model for the gamma-ray emission of binaries, a bold enterprise given current knowledge. While there is general agreement that anisotropic inverse Compton scattering of photons from the star and $\gamma\gamma$ pair production at TeV energies must play a role, since these processes naturally lead to orbital modulations, the details vary significantly from model to model. Modulated Doppler boosting is also very likely to intervene if the emission occurs in a pulsar wind bow shock. Reproducing the orbital phases of gamma-ray detections in systems with Be companions such as PSR B1259-63 has proven particularly difficult, possibly because of the complex interaction between the pulsar and the circumstellar material surrounding its companion. In the following, we adopted a simple model with the intention of minimizing the number of parameters while still being able to produce orbital lightcurves comparable to the observed ones.

4.1. Orbital parameters

The binary eccentricities e were assumed to follow the thermal distribution (Ambartsumian 1937) $p(e)de = 2ede$ with the additional conditions that $e < e_{\max} = 1 - (P_{\text{orb}}/2 \text{ days})^{-2/3}$ to ensure that the companion does not fill more than 70% of its Roche lobe at periastron and that the binaries are circularised ($e = 0$) for $P_{\text{orb}} \leq 2$ days (see Moe & Di Stefano 2017 and references therein). The inclination of the system is derived by randomly picking a vector on a sphere. The argument of periastron and the orbital phase at the time of the first simulated observation are picked from a uniform distribution between 0 and 2π . Finally, we uniformly sampled the logarithm of orbital periods between 1 and 10^4 days in order to assess the fraction of detected systems as a function of P_{orb} , except in §4.4 where this is slightly modified for a more realistic representation of the P_{orb} distribution of HMXBs.

4.2. Radiation model

We assume that the radiation is due to Compton upscattering of stellar photons with an initial energy ≈ 10 eV. GeV (resp. TeV) emission then requires electrons with a Lorentz factor $\gamma = 10^4$ (resp. $\gamma = 10^6$). For simplicity, we assumed monoenergetic distributions at these energies. This is supported by the observed GeV spectra of gamma-ray binaries, which generally consist of

a hard power-law with an exponential cutoff around 1 GeV. This is also admissible in the TeV range where soft power laws are observed so that most of the photons have an energy close the threshold energy of the VHE observations. The true particle distributions are likely to be more complex but the GeV and TeV emissions are dominated by electrons of these energies and assuming more complex distributions (power laws, see §5) does not have a significant impact on the results.

We computed the inverse Compton bolometric power radiated by these particles, assuming that they are located at the position of the compact object. If the electron distribution is isotropic, the lightcurve in the Thomson approximation for Compton scattering is given by

$$L_\gamma = N_e \sigma_T c U_\star (1 - \beta\mu) [(1 - \beta\mu)\gamma^2 - 1] \quad (1)$$

where $U_\star = (1/c)\sigma_{SB}T_\star^4(R_\star/d_\star)^2$ with T_\star the star temperature, R_\star its radius, d_\star its distance to the particles, and $\mu = \cos\theta$ represents the angle between the line-of-sight and the binary axis. The angle θ varies from $\pi/2 + i$ (superior conjunction) to $\pi/2 - i$ (inferior conjunction) with i the system inclination. The massive star was assumed to have a radius of $10R_\odot$ and temperature of 33,000 K. The analytic formula is valid for $\gamma = 10^4$, where the Thomson approximation is acceptable. However, stellar photons scatter in the Klein-Nishina regime when $\gamma = 10^6$. Hence, we numerically integrated the Compton kernel to derive the anisotropic emitted power instead of using Eq. 1 (see Dubus et al. 2010).

The total number of electrons N_e is related to the injected power in particles P_{inj} by

$$N_e = \frac{P_{\text{inj}}}{\gamma m_e c^2} \times \min\{\tau_{\text{esc}}, \tau_{\text{ic}}\} \quad (2)$$

where τ_{esc} is the escape timescale of the particles from the gamma-ray emitting region (see below) and τ_{ic} is the inverse Compton loss timescale, which in the Thomson regime is

$$\tau_{\text{ic}} = \frac{\gamma m_e c^2}{\frac{4}{3}\sigma_T c U_\star \gamma^2}. \quad (3)$$

Hence, $\langle L_\gamma \rangle = P_{\text{inj}}$ (integrated over all angles) if the particles radiate efficiently before they leave the vicinity of the star ($\tau_{\text{ic}} \leq \tau_{\text{esc}}$), otherwise the radiated power is reduced to the fraction of particles that are in the emission zone $\langle L_\gamma \rangle = (\tau_{\text{esc}}/\tau_{\text{ic}})P_{\text{inj}}$. Note that the latter can be rewritten using Kepler's third law as $L_\gamma \propto 1/d_\star \propto P_{\text{orb}}^{-2/3}$, hence there is a break in the distribution of $\langle L_\gamma \rangle / P_{\text{inj}}$ as a function of P_{orb} for the orbital period where $\tau_{\text{ic}} = \tau_{\text{esc}}$. This can be seen in Figure 3 where the mean of the average orbital luminosity is plotted for a sample of 10^4 binaries with orbital periods ranging from 1 to 10^4 days and randomly sampled eccentricities. The break is at $P_{\text{orb}} \approx 10$ days because we decided to set $\tau_{\text{esc}} = d_\star/c$. Such a fast escape timescale is reasonable in the context of gamma-ray binaries, where the accelerated particles flow away relativistically in a bow shock (Dubus et al. 2015). This assumption is also conservative in that it may underestimate the number of detections by minimizing the radiative efficiency. The influence of this choice on the results is further discussed in §5.2.

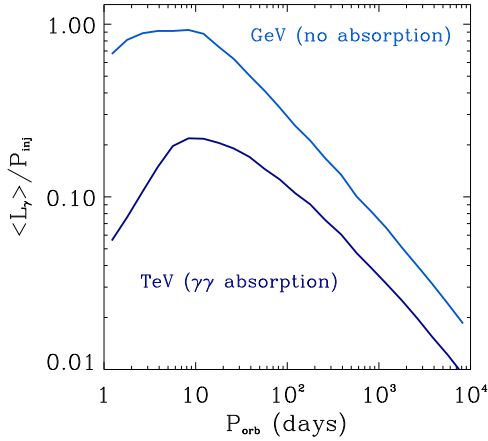
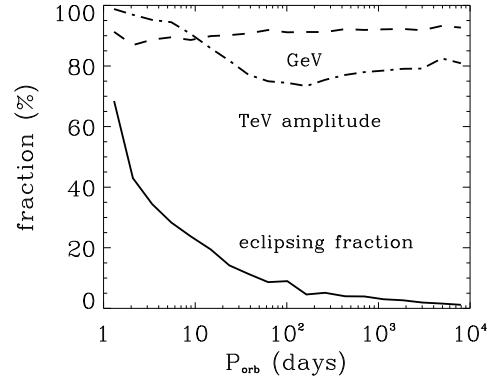
Since TeV photons are likely to create pairs by interacting with photons from the star, we calculated the expected $\gamma\gamma$ absorption at 1 TeV in the point source limit following Dubus (2006). Absorption reduces the average TeV luminosity for short orbital period systems, where the stellar radiation density is highest, resulting in a strong decrease of L_{TeV} with P_{orb} below 10 days (Fig. 3).

Table 3. Fraction of detected systems in each survey using the lightcurves in Fig. 1 as templates (see §3.3).

	LS 5039	LS I+61°303	PSR B1259-63	HESS J0632+057	1FGL J1018.6-5856	LMC P3
P_{orb} (days)	3.9	26.5	1236.7	315	16.5	10.3
eccentricity	0.35	0.54	0.87	0.83	—	—
distance (kpc)	2.9	2.0	2.3	1.6	5.4	50
$F_{\text{max,GeV}}$ (ph s ⁻¹)	4.2×10^{37}	2.1×10^{37}	2.0×10^{37}	2.9×10^{35}	1.0×10^{38}	5.4×10^{38}
$F_{\text{max,TeV}}$ (ph s ⁻¹)	1.9×10^{33}	1.4×10^{33}	1.1×10^{33}	2.5×10^{32}	1.5×10^{33}	—
<i>HE surveys (%)</i>						
FAVA	0.6 ± 0.2	1.4 ± 0.2	12.6 ± 0.7	< 0.1	8.0 ± 0.5	30.6 ± 0.9
3FGL	77.9 ± 0.8	67.1 ± 0.9	3.5 ± 0.4	0.8 ± 0.2	100	100
3FGL (extended)	100	97.3 ± 0.3	7.7 ± 0.5	1.9 ± 0.3	100	100
<i>VHE surveys (%)</i>						
HESS	10.3 ± 0.6	3.2 ± 0.4	1.5 ± 0.3	0.8 ± 0.2	5.2 ± 0.5	—
HAWC	7.7 ± 0.5	2.1 ± 0.3	0.4 ± 0.1	0.3 ± 0.1	4.0 ± 0.4	—
CTA	65.8 ± 0.9	23.7 ± 0.8	7.0 ± 0.5	5.1 ± 0.4	35.2 ± 0.9	—
CTA (full)	98.0 ± 0.3	47.0 ± 1.0	21.2 ± 0.8	11.2 ± 0.6	70.0 ± 0.9	—

Table 4. Fraction of detected systems in each survey using synthetic lightcurves as templates (see §4.3).

	LS 5039	LS I+61°303	PSR B1259-63	HESS J0632+057	1FGL J1018.6-5856	LMC P3
<i>HE surveys (%)</i>						
FAVA	0.9 ± 0.2	4.0 ± 0.4	10.7 ± 0.6	0.1 ± 0.1	16.7 ± 0.7	35.3 ± 1.0
3FGL	70.2 ± 0.9	39.9 ± 1.0	15.7 ± 0.7	0.3 ± 0.1	91.2 ± 0.6	99.7 ± 0.1
<i>VHE surveys (%)</i>						
HESS	7.5 ± 0.5	5.7 ± 0.5	1.6 ± 0.3	0.7 ± 0.2	7.0 ± 0.5	—
HAWC	5.2 ± 0.4	4.4 ± 0.4	0.8 ± 0.2	0.3 ± 0.1	5.4 ± 0.4	—
CTA	50.4 ± 1.0	38.3 ± 1.0	10.8 ± 0.6	3.7 ± 0.4	47.8 ± 1.0	—


Fig. 3. Mean orbit-averaged gamma-ray flux, normalized to the injected power, as a function of P_{orb} (see §4.2).

Fig. 4. Mean fractional amplitude of the simulated GeV (dashed line) and TeV (dash-dotted line) gamma-ray lightcurves (see Fig. 3) and fraction of the systems showing eclipses as a function of P_{orb} (thick line).

GeV emission is not affected by $\gamma\gamma$ absorption. However, we also took into account eclipses of the (point-like) gamma-ray emission zone by the star. This results in a slight decrease of the average GeV power at short P_{orb} , instead of the expected flat distribution $\langle L_\gamma \rangle = P_{\text{inj}}$. Hence, this model predicts the radiative efficiency is maximum for systems with $P_{\text{orb}} \approx 10$ days.

Figure 4 shows the average fractional amplitude of the model TeV lightcurves, measured as $(f_{\text{max}} - f_{\text{min}})/(f_{\text{max}} + f_{\text{min}})$, where

f is the flux. The mean amplitude increases slightly from short to long orbital periods due to the larger eccentricities permitted (see §4.1) but eclipses and $\gamma\gamma$ absorption strongly increase the amplitude at short P_{orb} . The average TeV variability amplitude at long P_{orb} is about 80%, implying $f_{\text{min}} \approx 0.11 f_{\text{max}}$. Fig. A.1 shows examples of GeV and TeV lightcurves computed using the radiative model described in this section.

4.3. Detectable fraction based on synthetic lightcurves

To check for consistency with the results of Table 3, we produced 10^4 synthetic lightcurves using the orbital period and eccentricity (when known) for each observed system *i.e.* leaving the system orientation free. We then normalized the synthetic lightcurves to the maximum observed luminosity. The systems are distributed throughout the Galaxy. The detection fractions in Table 4 are within a factor 2 or less of those in Table 3, showing comparable trends when looking at objects, orbital period or surveys. The exception is PSR B1259-63 where the detected fraction in the 3FGL-like survey is a factor 5 higher because the model typically produces a lower amplitude lightcurve than observed, hence a higher average flux (see below). Despite this shortcoming, our simple radiative model should still be able to yield realistic estimates of the average detection rate for a population of systems.

We then produced synthetic lightcurves for a sample of binaries with random orbital parameters and a given injected power. Figure 5 shows the fraction of systems detected in the mock HE and VHE surveys discussed in §2, as a function of P_{orb} and P_{inj} . The FAVA-like survey is much less efficient at detecting systems than the 3FGL-like survey. At short orbital periods, the sensitivity is insufficient to detect systems on a timespan of a week. At long orbital periods, the amplitude of the variations in the model lightcurves (Fig. 4) is insufficient to provide a significant advantage to this ‘burst’ search strategy compared to the ‘integration’ strategy employed in the 3FGL-like survey. The latter is extremely efficient when the injected power in HE-emitting particles exceeds $10^{35} \text{ erg s}^{-1}$, even for long P_{orb} compared to the integration time (4 years).

The VHE surveys access only part of the Galactic Plane so their maximum efficiency does not reach 100% even for high injected powers in VHE-emitting particles. The results show comparable efficiencies for the HESS and HAWC-like surveys. The design of these two surveys, notably the visit frequencies, does not appear to play a major role in the detectable fraction: the peak at $P_{\text{orb}} \approx 10$ to 100 days simply reflects the higher radiated luminosity expected for those orbital periods in the model (see Fig. 3). The CTA-like survey is much more sensitive, detecting nearly all accessible systems for $P_{\text{inj}} \geq 10^{35} \text{ erg s}^{-1}$ regardless of orbital period. Again, the sensitivity at long P_{orb} results from our model, which on average gives a minimum flux around 11% of the maximum flux (Fig. 4 and §4.2). This enables the detection of long orbital period systems even when the phases of maximum flux are not sampled by the visits.

4.4. Full population model

A full population model requires assumptions on the injected power P_{inj} and how it relates to the total available power \dot{E} measured by pulsar spindown. P_{inj} is likely to be different for the GeV and TeV emitting particles, whether they arise from different populations or from the same power-law distribution. We used PSR B1259-63, the only system with a measured $\dot{E} = 8 \times 10^{35} \text{ erg s}^{-1}$, to estimate the power going to the GeV and TeV-emitting particles. Simulating GeV and TeV lightcurves with the same orbital period and eccentricity as PSR B1259-63 (*i.e.* following the procedure described in §4.3), we found that injection fractions $P_{\text{GeV}} = 0.07\dot{E}$ and $P_{\text{TeV}} = 0.01\dot{E}$ are needed to reproduce, on average, the peak gamma-ray fluxes listed in Tab. 3 and adopted these values in the following.

The mock population is built by randomly sampling probability distributions of \dot{E} and P_{orb} . Following Lutovinov et al. (2013), we took a flat distribution in $\log P_{\text{orb}}$ tapered by gaus-

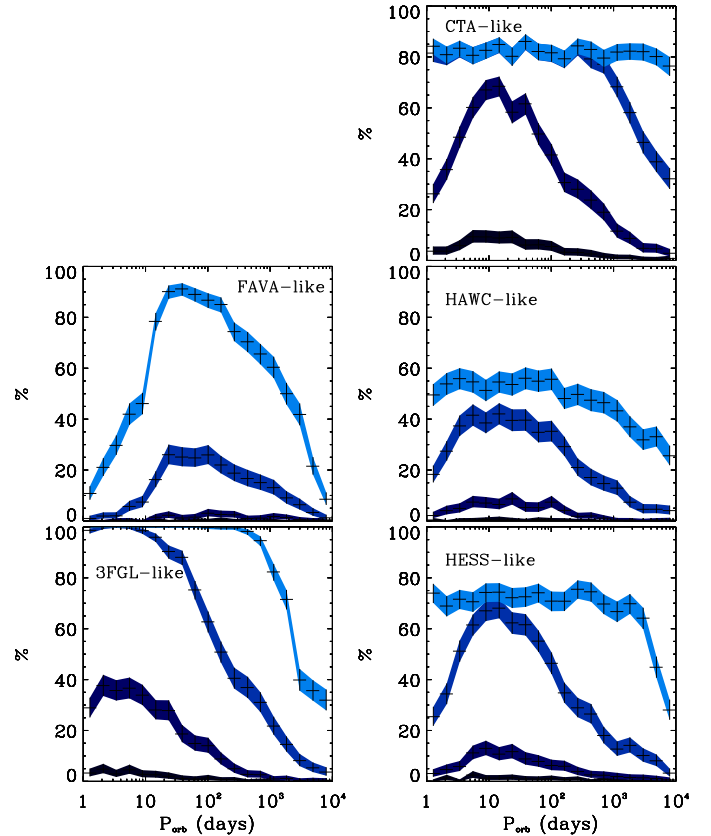


Fig. 5. Detected fractions in the HE (left panels) and VHE (right panels) surveys. Each panel contains four curves corresponding to $P_{\text{inj}} = 10^{33}, 10^{34}, 10^{35}, 10^{36} \text{ erg/s}$ (dark to light blue sequence in each panel). The detection fraction increases when going from small P_{inj} (darker blue) to high P_{inj} (lighter blue) until the detected fraction saturates at the value given by the observable fraction (Tab. 2).

sian edges at $\log P_{\text{orb}} (\text{days}) = 1.3$ and 3.7 . This probability distribution (Fig. 6, top left panel) results from the evolution of pre-HMXB binaries (Bhadkamkar & Ghosh 2012). For \dot{E} , we took as input the distribution of spindown powers extracted from the ATNF pulsar catalogue (Manchester et al. 2005)⁶, selecting only those pulsars with a pulse period $> 10 \text{ ms}$ and a spindown timescale $< 10^7 \text{ year}$ to exclude recycled millisecond pulsars. The resulting \dot{E} distribution is shown in the top right panel of Fig. 6.

The detection fraction in the various surveys is calculated from a random sample of 10^5 systems (Tab. 5). The distributions of detected systems in present-day or future surveys are shown in the zoomed-in bottom panels of Fig. 6. The detection fractions are biased towards short P_{orb} and high \dot{E} , as expected from the results of §4.3. The population model naturally accounts for the existence of radio pulsars in binaries that remain undetected in gamma rays due to their long orbital periods and low spindown powers. PSR J0045-7319, PSR J1638-4725, PSR J1740-3052 with $P_{\text{orb}} = 51, 1941, 231 \text{ days}$ (resp.) and $\dot{E} = 0.2, 0.4, \text{ and } 5 \times 10^{33} \text{ erg s}^{-1}$ (resp.) are examples of such systems that we do not expect to be readily detectable by the gamma-ray surveys (Stairs et al. 2001; Bassa et al. 2011; Madsen et al. 2012).

The pulsar wind pressure can be insufficient to hold off accretion from the companion’s stellar wind for low \dot{E} and short P_{orb} , in which case we consider that the system will be an accreting

⁶ <http://www.atnf.csiro.au/people/pulsar/psrcat/>

Table 5. Detection fractions for the population shown in Fig. 6.

mock survey	detection fraction (%)
3FGL or FAVA	4.83±0.13
FAVA	1.96±0.09
3FGL	4.73±0.13
3FGL (extended)	6.21±0.15
HESS	1.17±0.07
HAWC	0.88±0.06
CTA	3.78±0.12
CTA (full)	5.83±0.15

HMXB (or a propeller, depending on the respective locations of the co-rotation radius and magnetospheric radius, both of which are within the light cylinder) and will not emit gamma rays. We used a simple criterion to test whether a system is accreting or not, assuming the massive star wind is isotropic, uniform with the same constant mass loss rate $\dot{M}_w = 10^{-6} M_\odot \text{ yr}^{-1}$ and velocity $v_w = 1000 \text{ km s}^{-1}$ for all systems. The system is accreting if the pulsar spindown power is less than

$$\dot{E} < 4 \cdot 10^{33} \left(\frac{\dot{M}_w}{10^{-6} M_\odot \text{ yr}^{-1}} \right) \left(\frac{10^3 \text{ km s}^{-1}}{v_w} \right)^3 \left(\frac{0.1 \text{ AU}}{a_p} \right)^2 \text{ erg s}^{-1} \quad (4)$$

where a_p is the binary separation at periastron (Illarionov & Sunyaev 1975). This criterion is simplistic in regards to the complex physics of wind launching, capture, Be circumstellar discs etc (Dubus 2013), but we have chosen values of \dot{M}_w and v_w that are likely to overestimate the fraction of accreting systems. We find about 23% of the sampled systems are accreting, mostly at short P_{orb} and low \dot{E} as shown by the line-filled histogram in the top panels of Fig. 6. Despite this, we find negligible overlap with the population of systems detected in the HE and VHE surveys because these select high \dot{E} systems (< 0.4% of the detected systems are also flagged as accreting).

About 40% of the binaries that are detected in HE can be found in both the 3FGL and FAVA-like surveys whereas less than 2% are detected only in the FAVA-like survey. The detection of PSR B1259-63 in FAVA without a concurrent detection in the 3FGL survey is therefore unlikely in our model, as the statistics in §4.3 already showed. However, PSR B1259-63 is close to our crude 3FGL detection threshold using the template lightcurve so details in the 3FGL detectability may come into play (orbit-to-orbit fluctuations, Galactic diffuse emission). The probability to detect a system in one of the VHE surveys (HESS, HAWC and CTA-like) is $4.23 \pm 0.13\%$, with most of the detections arising from the CTA-like survey. Altogether, the probability to detect a gamma-ray binary in any of the surveys is $5.32 \pm 0.14\%$ (3FGL, FAVA, HESS, HAWC, or CTA-like). Only a very small number are detected in VHE surveys without a detection in the HE surveys with this model. For instance, all of the systems detected by the HESS-like survey are also detected by the 3FGL-like survey.

5. Discussion

5.1. Estimated population of gamma-ray binaries

We explored two ways to estimate the number of gamma-ray binaries. The first (§3.3) employed the lightcurves of the known systems as templates to evaluate the detection probability of identical systems distributed throughout the Galaxy. The results

show that systems like LS 5039, LS I +61°303, LMC P3 and 1FGL J1018.6-5856 are already detectable throughout most of the Galaxy, so it is highly unlikely that more than 1 or 2 have escaped notice (Tab. 3). Future HE detections are more likely to be of low duty cycle systems like PSR B1259-63, the total number of which is estimated at 7_{-6}^{+26} . One such anticipated detection is that of PSR J2032+4127, a $2 \times 10^{35} \text{ erg s}^{-1}$ pulsar in an eccentric, >20 year orbit around a Be star that will pass periastron in late 2017 (Lyne et al. 2015; Ho et al. 2017)⁷. The largest source of uncertainty is the number of HESS J0632+057-like systems with a ratio of TeV to GeV luminosity about two order-of-magnitude higher than the other binaries (see Tab. 3 and Li et al. 2017). There may be as many as ≈ 230 such systems in our Galaxy, an upper limit that CTA will decrease to 8_{-7}^{+30} if none are discovered in the full Galactic Plane survey (§3.3).

The known systems represent only the upper end of the luminosity function of gamma-ray binaries. Thus, our second estimate for the number of gamma-ray binaries employed a full population model based on a series of assumptions on the radiative process, the distributions of orbital parameters and injected power (§4). In the HE domain, with four systems in the 3FGL and FAVA surveys (Tab. 1, excluding LMC P3 since it is not in the Galactic Plane), the total parent population is estimated at 82_{-56}^{+108} systems based on the detection fraction in Tab. 5. In the VHE domain, with only LS 5039 detected in the HESS survey, the parent population is constrained to 85_{-81}^{+290} systems. Combining all the information in Tab. 1 into the likelihood function, *i.e.* assuming four systems in the HE surveys, one system in HESS, none in HAWC, and at least five in the full CTA survey, the population is estimated at 101_{-52}^{+89} gamma-ray binaries in our Galaxy. These numbers are consistent with the predictions from population synthesis of HMXBs (§1).

Gamma-ray surveys are $\geq 50\%$ complete for $\dot{E} \geq 10^{36} \text{ erg s}^{-1}$ (Fig. 6), but they access only a handful of systems in a population of about a hundred binaries. A few additional systems like PSR J2032+4127 may be detected through their pulsed gamma-ray emission without showing binary-related gamma-ray emission. We have not attempted to take this into account. The spindown distribution of detected *Fermi*-LAT pulsars peaks at $\log \dot{E} = 35.5$ (see §5.2 below) suggesting this is unlikely to make a difference to the number of systems detected in gamma rays. A couple dozen binaries may be visible as accreting X-ray sources, indistinguishable from other HMXBs except perhaps through their neutron star spin periods or through propeller-induced behaviour. SAX J0635+0533 (Cusumano et al. 2000) and A0538-66 (Skinner et al. 1982) are possible examples. These two systems clearly have much faster spin periods (< 70 ms) than all the other known X-ray pulsars in HMXBs (> 1 to 1000s), suggesting that the neutron star may not yet have spun down significantly from its birth period.

PSR J0045-7319, PSR J1638-4725, and PSR J1740-3052 are representative of the low \dot{E} systems that represent the majority of the pulsar + massive star population: $\approx 55\%$ of the sampled systems have $\dot{E} \leq 10^{34} \text{ erg s}^{-1}$ and are not accreting. Adding in the 23% that are accreting, this implies that 78% of the population is inaccessible to gamma-ray surveys. Estimating their detection rate in radio (SKA) or X-ray surveys (eROSITA) is beyond the scope of this work but we note that the long P_{orb} , high eccentricity systems are clearly more susceptible to be detected as radio

⁷ PSR J2032+4127 is a *pulsed Fermi*-LAT source and coincident with an extended, persistent VHE source. It does not yet show evidence for variable gamma-ray emission related to binary motion, as seen in PSR B1259-63 and the other gamma-ray binaries.

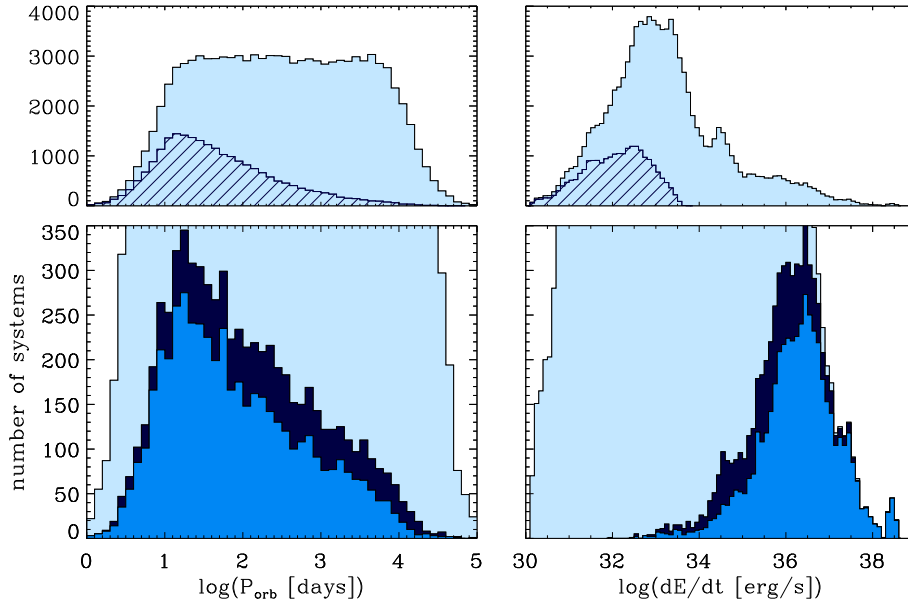


Fig. 6. Orbital period (left panels) and spindown power distribution (right panels) of a random sample of 10^5 systems. Top panels show the full population as a light blue histogram with the line-filled fraction showing the distribution of the binaries that are accreting according to Eq. 4. The bottom panels zoom in to highlight the systems detected in any of the present-day surveys (combining the HESS, 3FGL and FAVA-like surveys, medium blue histogram) or any of the future surveys (combining the full CTA, extended 3FGL and HAWC-like surveys, dark blue histogram). The latter essentially shows the systems detected in any survey since a binary detected in one of the present-day surveys has a nearly >99% chance of being re-detected in one of the future surveys.

pulsars (Lipunov et al. 1994), providing a complementary way to access the pulsar + massive star population.

5.2. Systematic uncertainties in the population synthesis

How dependent are our results on the assumptions of the model? The Galactic distribution and binary parameters should not be a major source of concern since these have already been scrutinized in population studies of high-mass X-ray binaries (Walter et al. 2015). The distribution of \dot{E} for gamma-ray binaries is entirely unknown and taking as input the \dot{E} distribution of young pulsars in the ATNF catalog probably suffers from a variety of selection biases, notably because it is not obvious that the birth spin period and evolution should be identical in isolated pulsars and binaries (if only because mass loss and kick during the supernova are necessarily weaker if the newly-born neutron star is to remain bound to its companion). Yet, our assumption on \dot{E} is not likely to have a major impact on gamma-ray observations since these are mostly sensitive to the high end of this distribution. The \dot{E} distribution of detected binaries (Fig. 5) actually resembles the \dot{E} distribution of young pulsars detected in gamma-rays with the *Fermi*-LAT⁸, which we find to be well-approximated by a Gaussian centered at $\log \dot{E} = 35.5$ with a standard deviation $\sigma = 1$. Taking this distribution as input increases the detection fraction, decreasing the population size inferred from current observations without changing much the number of expected detections in future surveys. However, this distribution cannot account for the known radio pulsars in orbit around massive stars with low \dot{E} . The strongest impact of our assumption on the \dot{E} distribution is therefore on the relative numbers of pulsar+massive star binaries that are found in radio and gamma-ray surveys.

⁸ [link](#) to the public list of LAT-detected gamma-ray pulsars

The lightcurves of gamma-ray binaries have proven difficult to model, even in the cases where we have the most information, questioning the validity of our radiative model. For instance, relativistic beaming of the emission is thought to be an important factor in shaping the lightcurves (e.g. An & Romani 2017). A refined lightcurve model is desirable but may not change our results much. First, despite its simplicity, the detection fractions inferred from the model are broadly consistent with those inferred from the observed lightcurves (§3.1). Its main shortcoming is that it predicts lower amplitudes than observed, overestimating detection rates for PSR B1259-63-like systems. However, these do not dominate the detected systems (Fig. 6). Second, we have experimented with a more complex radiative model, using a power-law distribution of particles and including Doppler boosting (assuming a particle bulk velocity of $c/3$ directed away from the star as in Dubus et al. 2010). There was surprisingly little difference with the detection fractions shown in Fig. 5 despite substantial changes to the lightcurves from relativistic Doppler boosting, indicating that the flux level is more important than the detailed shape of the lightcurve in setting the detection fractions.

Improvements to our radiative model should thus concentrate on the injected power P_{inj} and the radiative efficiency $\tau_{\text{esc}}/\tau_{\text{ic}}$, both of which set the flux level. A longer escape timescale increases the radiative efficiency but this needs to be compensated by a lower fraction P_{inj}/\dot{E} in order to match the maximum flux from PSR B1259-63 (§4.4). For example, taking $\tau_{\text{esc}} = 10d/c$ implies a decreased injection fraction ($P_{\text{GeV}} \approx 0.02\dot{E}$ and $P_{\text{TeV}} \approx 0.002\dot{E}$). The combination yields an estimated population of 105^{+92}_{-54} systems, very close to our previous estimate of 101^{+89}_{-52} . The peak of the gamma-ray flux distribution is pushed to longer periods than in Fig. 3, leading to a flatter distribution in the fraction of detected systems as a function of P_{orb} . In principle,

the P_{orb} distribution of detected gamma-ray binaries could thus be used to constrain τ_{esc} , assuming excellent knowledge of their parent P_{orb} distribution. A distribution of L_{γ}/\dot{E} as a function of P_{orb} would narrow down possibilities for the radiative and injection efficiency, presently only constrained by observations of PSR B1259-63. Gamma-ray observations of PSR J2032+4127 at periastron passage will provide a second constrain on these efficiencies. Inversely, future observations of gamma-ray binaries as a population also have the potential to constrain the relative efficiencies in the GeV and TeV range, as described below (§5.3).

Many of our results remain applicable even if gamma-ray binaries are not powered by pulsar spindown. The results of §3, based on the template lightcurves, do not depend on this assumption. The results of §4.1-4.3 are also applicable as long as the emission arises from electrons located close to the compact object (e.g. at the base of a jet) upscattering stellar radiation. Even if the compact object is a black hole, the compact object mass remains much lower than the companion mass so any difference in orbits will be minor for the radiation model. However, differences can be expected in the full population model (§4.4) since we have made use of the distribution of spindown powers of pulsars. We would need some assumption on the distribution of jet power to perform an equivalent calculation and deduce the parent population. However, as stated in the introduction, we consider it very unlikely that gamma-ray binary emission arises from accretion-powered jets (Dubus 2013).

5.3. Future gamma-ray observations

What do future observations hold in store? With an estimated population size of 101 gamma-ray binaries, up to 8 new binaries might be detected in an extended 3FGL survey with a most likely value of 2 new detections beyond the known sample. New discoveries are less likely in the VHE surveys. Once the expected detections (Tab. 1) are taken into account, up to 3 new detections are predicted in the HAWC survey, 5 in the initial CTA survey and 6 in the full CTA survey (95% confidence limits), the statistically most likely outcome being no new detection. The reason is that the detection probabilities remain small for these surveys.

Serendipitous discoveries in deep VHE observations of Galactic sources (e.g. HESS J0632+057) can complement the surveys. We find that the probability for a chance detection of a gamma-ray binary is $0.17 \pm 0.03\%$ in a 100 hour CTA exposure towards the Galactic Center, covering 6° in Galactic longitude, and reaching 1 mCrab at 1 TeV. This is ≈ 1.7 times the detection rate from the Galactic Plane survey over a comparable area *i.e.* there are roughly 7 previously undetected systems for every 10 systems detected in the Galactic Plane survey of this deep field. Having 20 such deep pointings, spread around the Galactic Plane towards areas of special interest such as the Galactic Center, the Cygnus and Westerlund regions, or the Sagittarius-Carina spiral arm (see Fig. 2), adds 1.4% to the detected fraction with CTA. Combining surveys and deep pointings can thus yield a detection rate comparable to or greater than that in the *Fermi*-LAT survey.

Any discovery in a VHE survey would have a major impact on the estimated population number, raising it to higher values. A discrepancy could appear between the actual number of sources detected in the VHE and HE surveys since the model predicts that essentially all TeV sources should be detected at GeV energies. Some tension is already present in the model. The maximum likelihood L_m obtained by treating independently the HE and VHE surveys is $\geq 20\%$ for both, with corresponding population numbers of 82^{+108}_{-56} (HE) and 132^{+268}_{-86} (VHE). Combining the HE and VHE numbers into a single likelihood gives the estimate

of 101^{+89}_{-52} systems presented above, but L_m drops to 4%: this low probability indicates that the model has difficulty accounting for both the number of GeV and TeV detections when they are taken from the same underlying binary population. This can be resolved by increasing the injection fraction P_{inj} at 1 TeV, with the effect of raising the detection probability in VHE surveys and lowering the parent population size to a value that slackens the tension with the HE constraints, or by lowering it at 1 GeV with opposite effects on detection probability and population size. Hence, the relative numbers of HE and VHE detections can constrain the relative injection efficiencies. In any case, regardless of the value of P_{inj} , the population of VHE-emitting systems is unlikely to be greater than 230 systems, otherwise HESS J0632+057-like systems would be detected in the 3FGL survey or in the HESS Galactic Plane survey (§3.3). This number is close to the upper limit on the population size estimated from synthetic lightcurves (190 systems). Both estimates thus converge to a maximum gamma-ray binary population of ≈ 200 systems. With 200 systems, up to 10 (resp. 14) new binaries could be detected in the initial (resp. full) CTA survey, the most likely number being 4 (resp. 6) discoveries.

6. Conclusions

We have modelled the population of gamma-ray binaries and evaluated the fraction of systems that can be detected in various HE and VHE surveys, taking into account the variability of their gamma-ray emission. The number of gamma-ray binaries is constrained to 101^{+89}_{-52} systems in our Galaxy. This number matches expectations from HMXB population synthesis.

Gamma-ray binaries are rare systems and we do not expect a watershed of discoveries in the near future. Pursuing the *Fermi*-LAT survey to ≈ 2024 should lead to a handful of discoveries, mostly PSR B1259-63-like systems. At very high energies, combining Galactic Plane surveys and deep observations of Galactic sources with CTA should provide a comparable number of discoveries. However, the number of HESS J0632+057-like systems, with very weak GeV emission, is a major source of uncertainty. Observations already indicate that the GeV and TeV emission originate from different particle populations. A VHE survey could therefore reveal a population of binaries that cannot be seen with the *Fermi*-LAT. Such a population is limited to $\lesssim 230$ systems based on the lack of HESS J0632+057-like systems in the *Fermi*-LAT 3FGL survey and the HESS Galactic Plane Survey. With 200 systems, four new gamma-ray binaries can be expected in the first two years of the CTA Galactic Plane survey. Of course, these numbers refer only to gamma-ray binaries and do not limit gamma-ray detections from other types of binaries such as novae, colliding wind binaries, binary millisecond pulsars, microquasars, etc.

Detecting a system depends more on its orbit-averaged flux than on the shape of the gamma-ray lightcurve. Thus, the scheduling of visits from ground-based instruments plays a minor role in setting the detected fraction. The average flux is set by the efficiency with which spindown power is radiated in the HE and VHE bands. This is the most important source of uncertainty in our model. Ideally, this should be constrained by measuring the pulsar spindown power and radiated luminosity for as many systems as possible. At present, this is limited to PSR B1259-63, with the possible addition of PSR J2032+4127 in the near future. Alternatively, this relative efficiency in the HE and VHE bands can be constrained statistically by the relative number of sources detected in HE and VHE surveys.

About 55% of pulsars in orbit around massive stars are hardly accessible to gamma-ray observations, which are most sensitive to the high \dot{E} , short P_{orb} systems. Low \dot{E} and long P_{orb} binaries are likely to be more efficiently accessed by radio pulsar surveys, which are thus fully complementary to the gamma-ray observations. Another significant fraction, $\approx 23\%$, may actually be visible as accreting X-ray pulsars or propellers instead of binary pulsar wind nebulae. Future work should strive to combine detection probabilities in gamma rays with detection probabilities in radio (SKA) and X-ray (eROSITA) surveys.

Acknowledgements. We are grateful to Masha Chernyakova, Markus Böttcher, and Jamie Holder for their careful CTA internal review that helped improve this work. GD and POP acknowledge support from *Centre National d'Etudes Spatiales* (CNES).

This paper has gone through internal review by the CTA Consortium.

Appendix A: Example synthetic lightcurves

References

- Abdo, A. A., et al. (*Fermi*-LAT collaboration) 2009, *ApJ*, 706, L56
- Abdollahi, S., et al. (*Fermi*-LAT collaboration) 2016, *ApJS*, submitted [arXiv:1612.03165]
- Abeyssekara, A. U., et al. (HAWC collaboration) 2017, *ApJ*, 843, 40
- Abramowski, A., et al. (HESS collaboration) 2015, *A&A*, 577, A131
- Acciari, V. A., et al. (VERITAS collaboration) 2011, *ApJ*, 738, 3
- Acero, F., et al. (*Fermi*-LAT collaboration) 2015, *ApJS*, 218, 23
- Ackermann, M., et al. (*Fermi*-LAT collaboration) 2013, *ApJ*, 773, L35
- Ackermann, M. et al. (*Fermi*-LAT collaboration) 2012, *Science*, 335, 189
- Aharonian, F. A., et al. (HESS collaboration) 2006, *A&A*, 460, 743
- Albert, J., et al. (MAGIC collaboration) 2008, *ApJ*, 674, 1037
- Aliu, E., et al. (VERITAS and HESS collaborations) 2014, *ApJ*, 780, 168
- Ambartsumian, V. A. 1937, *Astron. Zhurn.*, 14, 207
- An, H. & Romani, R. W. 2017, *ApJ*, 838, 145
- Bassa, C. G., Briske, W. F., Nelemans, G., et al. 2011, *MNRAS*, 412, L63
- Bhadkamkar, H. & Ghosh, P. 2012, *ApJ*, 746, 22
- Bordas, P., Dubus, G., Eger, P., et al., 2017, in 6th International Meeting on High-energy gamma-ray astronomy, AIP Conference Proceedings, 1792, 040017
- Campana, S., Stella, L., Mereghetti, S., & Colpi, M. 1995, *A&A*, 297, 385
- Carramiñana, A. 2016, *Journal of Physics Conference Series*, 761, 012034
- Corbet, R. H. D., Chomiuk, L., Coe, M. J., et al. 2016, *ApJ*, 829, 105
- Cusumano, G., Maccarone, M. C., Nicastro, L., Sacco, B., & Kaaret, P. 2000, *ApJ*, 528, L25
- Dubus, G. 2006, *A&A*, 451, 9
- Dubus, G. 2013, *A&A Rev.*, 21, 64
- Dubus, G., Cerutti, B., & Henri, G. 2010, *A&A*, 516, A18
- Dubus, G., Lamberts, A., & Fromang, S. 2015, *A&A*, 581, A27
- Gregory, P. C. & Taylor, A. R. 1978, *Nature*, 272, 704
- Grimm, H.-J., Gilfanov, M., & Sunyaev, R. 2002, *A&A*, 391, 923
- Hadasch, D., Torres, D. F., Tanaka, T., et al. 2012, *ApJ*, 749, 54
- Hinton, J. A., Skilton, J. L., Funk, S., et al. 2009, *ApJ*, 690, L101
- Ho, W. C. G., Ng, C.-Y., Lyne, A. G., et al. 2017, *MNRAS*, 464, 1211
- Iben, I. J., Tutukov, A. V., & Yungelson, L. R. 1995, *ApJS*, 100, 217
- Illarionov, A. F. & Sunyaev, R. A. 1975, *A&A*, 39, 185
- Johnston, S., Manchester, R. N., Lyne, A. G., et al. 1992, *ApJ*, 387, L37
- Li, J., Torres, D. F., Cheng, K.-S., et al. 2017, *ApJ*, accepted [arXiv:1707.04280]
- Lipunov, V. M., Nazin, S. N., Osminkin, E. Y., & Prokhorov, M. E. 1994, *A&A*, 282, 61
- Lutovinov, A. A., Revnivtsev, M. G., Tsygankov, S. S., & Krivonos, R. A. 2013, *MNRAS*, 431, 327
- Lyne, A. G., Stappers, B. W., Keith, M. J., et al. 2015, *MNRAS*, 451, 581
- Madsen, E. C., Stairs, I. H., Kramer, M., et al. 2012, *MNRAS*, 425, 2378
- Malyshev, D. & Chernyakova, M. 2016, *MNRAS*, 463, 3074
- Manchester, R. N., Hobbs, G. B., Teoh, A., & Hobbs, M. 2005, *AJ*, 129, 1993
- Massi, M., Migliari, S., & Chernyakova, M. 2017, *MNRAS*, in press [arXiv:1704.01335]
- Meurs, E. J. A. & van den Heuvel, E. P. J. 1989, *A&A*, 226, 88
- Moe, M. & Di Stefano, R. 2017, *ApJS*, 230, 15
- Paredes, J. M., Martí, J., Ribó, M., & Massi, M. 2000, *Science*, 288, 2340
- Portegies Zwart, S. F. & Verbunt, F. 1996, *A&A*, 309, 179
- Portegies Zwart, S. F. & Yungelson, L. R. 1998, *A&A*, 332, 173
- Ringermacher, H. I. & Mead, L. R. 2009, *MNRAS*, 397, 164
- Russek, D. 2003, *A&A*, 397, 133
- Shvartsman, V. F. 1971, *Soviet Astronomy*, 15, 342
- Skinner, G. K., Bedford, D. K., Elsner, R. F., et al. 1982, *Nature*, 297, 568
- Stairs, I. H., Manchester, R. N., Lyne, A. G., et al. 2001, *MNRAS*, 325, 979
- Tauris, T. M. & van den Heuvel, E. P. J. 2006, in *Compact stellar X-ray sources*, ed. W. H. G. Lewin & M. van der Klis (Cambridge Astrophysics Series, No. 39, Cambridge, UK: Cambridge University Press), 623–665
- Vercellone, S. 2017, in 6th International Meeting on High-Energy Gamma-Ray Astronomy, AIP Conference Proceedings, 1792, 030001
- Walter, R., Lutovinov, A. A., Bozzo, E., & Tsygankov, S. S. 2015, *A&A Rev.*, 23, 2

List of Objects

- ‘LS I +61°303’ on page 1
- ‘1FGL J1018.6-5856’ on page 1
- ‘LS 5039’ on page 1
- ‘LMC P3’ on page 1
- ‘HESS J0632+057’ on page 1
- ‘PSR B1259-63’ on page 1
- ‘PSR J0045-7319’ on page 1
- ‘PSR J1638-4725’ on page 1
- ‘PSR J1740-3052’ on page 1
- ‘PSR J2032+4127’ on page 1
- ‘SAX J0635+0533’ on page 9
- ‘A0538-66’ on page 9

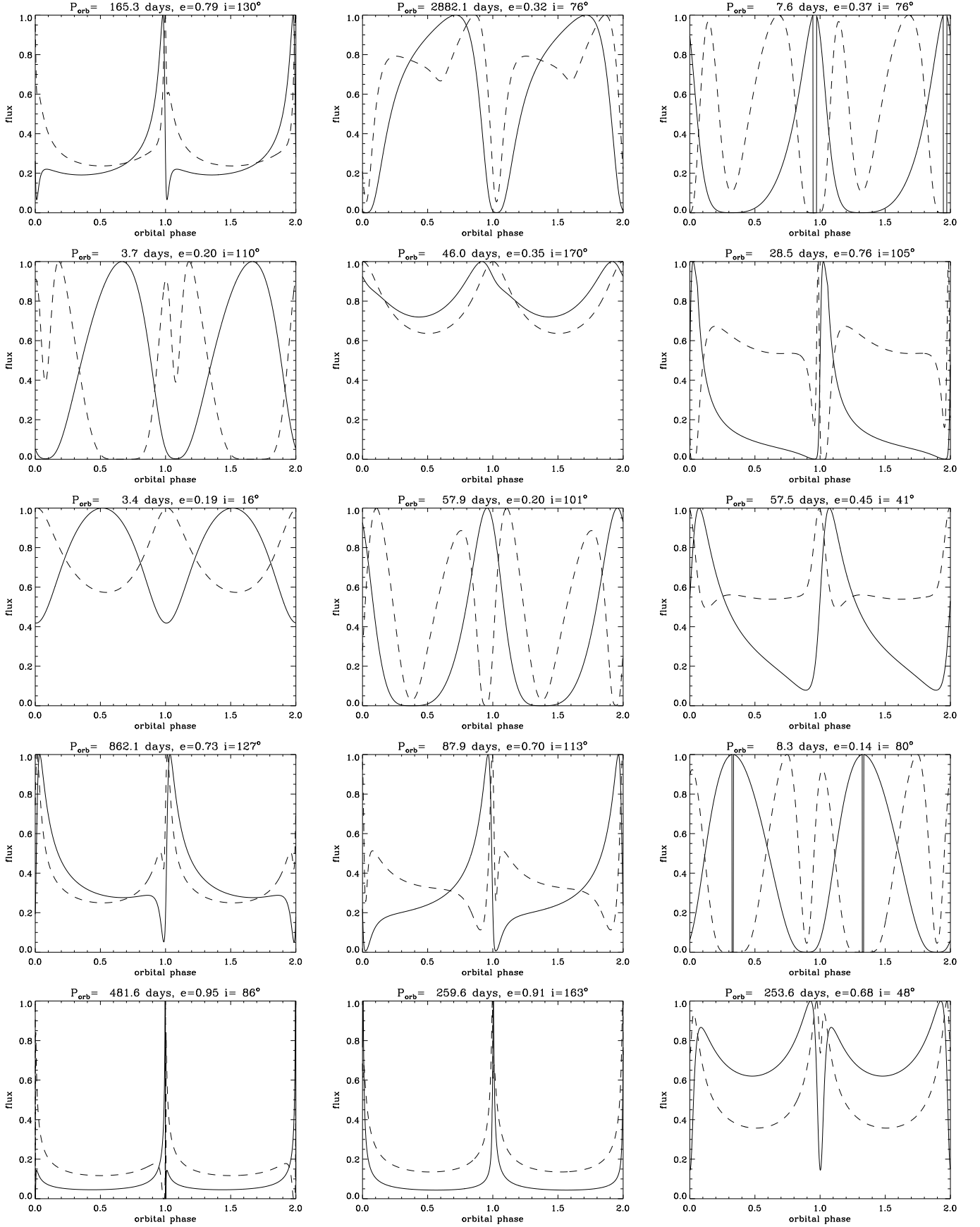


Fig. A.1. Example lightcurves computed from the model described in §4.2 (full line: GeV emission; dashed line: TeV emission, taking into account $\gamma\gamma$ absorption). The orbital period and eccentricity of the binary system is indicated in the title of each plot. The lightcurves are normalised to the maximum value. The systems shown here are a random selection of the systems flagged as detected in Fig. 6. Periastron passage is at phase 0.